Supporting Information for

Perylenothiophene Diimides: Physicochemical Properties and Applications in Organic Semiconducting Devices

Masahiro Nakano,[a*] Kyohei Nakano,[b] Kazuo Takimiya,[a,c*] Keisuke Tajima[b]

[a]Emergent Molecular Function Research Group, RIKEN Center for Emergent Matter Science (CEMS), 2-1, Hirosawa, Wako, Saitama, 351-0198, Japan.
[b]Emergent Functional Polymers Research Team, RIKEN Center for Emergent Matter Science (CEMS), 2-1, Hirosawa, Wako, Saitama, 351-0198, Japan.
[c]Department of Chemistry, Graduate School of Science, Tohoku University, 6-3, Aoba, Aramaki, Aoba-ku, Sendai, 980-8578, Japan.

Contents

1. Synthesis of mono-halogenated PDIs

N,*N*′-Bis(1-penthylhexyl)-1-bromoperylene-3,4,9,10-tetracarboxydiimide (**1a**)[1] and *N*,*N*′-bis(1-pentylhexyl)-2-iodoperylene-3,4,9,10-tetracarboxydiimide (**1b**)[2] were synthesized from *N*,*N*′-bis(1-penthylhexyl)-perylene-3,4,9,10-tetracarboxydiimide[3] according to the reported procedures.

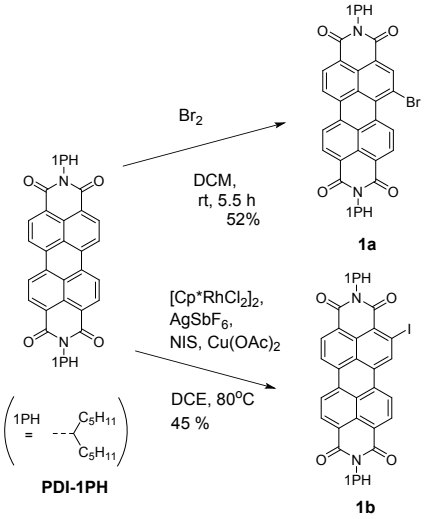

Scheme S1. Synthesis of **1a** and **1b**.

***N*,*N*′-Bis(1-penthylhexyl)-1-bromoperylene-3,4,9,10-tetracarboxydiimide (1a)**

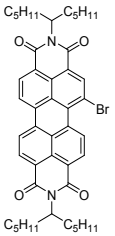

A mixture of *N*,*N*′-bis(1-penthylhexyl)-perylene-3,4,9,10-tetracarboxydiimide (3.86 g, 5.52 mmol) and bromine (33.7 g, 212 mmol) in 108 mL of dichloromethane was stirred at rt for 2 days. The mixture was quenched with diluted $NaHSO_3$ aqueous solution (30 mL) and extracted with dichloromethane (100 mL). Then, the solvent was evaporated and the residue was purified by column chromatography on silica gel eluted with dichloromethane/hexane (1:1, v/v) to give **1a** as an orange

solid (4.60 g, 52%): ^{1}H NMR (400 MHz, $CDCl_3$): δ 9.79 (d, *J* = 8.0 Hz, 1H), 8.91 (s, 1H), 8.69–8.67 (m, 3H), 8.59–8.57 (m, 2H), 5.22–5.12 (m, 2H), 2.31–2.21 (m, 4H), 1.94–1.85 (m, 4H), 1.43–1.21 (m, 24H), 0.84 (t, *J* = 6.8 Hz, 6H), 0.83 (t, *J* = 6.8 Hz, 12H); ^{13}C NMR (100 MHz, $CDCl_3$): 163.9, 163.8, 163.1, 162.8, 139.2, 134.0, 133.7, 133.6, 131.1, 130.61, 130.55, 129.1, 128.9, 128.3, 128.2, 128.1, 127.2, 124.1, 124.0, 123.7, 123.3, 122,9, 122.6, 121.0, 55.1, 54.9, 32.5, 32.4, 31.74, 31.72, 26.63, 26.61, 22.5, 13.9; IR (KBr) ν = 1701, 1661 cm^{-1} (C=O); MP: 198.2–198.7 °C; HRMS (APCI) m/z calcd for $C_{46}H_{53}BrN_2O_4$: $[M]^+$ 777.3267. Found: 777.3263.

_N_,_N_′-Bis(1-pentylhexyl)-2-iodoperylene-3,4,9,10-tetracarboxydiimide (1b)

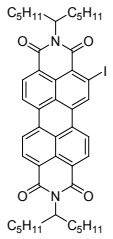

A mixture of $[Cp^*RhCl_2]_2$ (152 mg, 0.248 mmol) and $AgSbF_6$ (564 mg, 1.63 mmol) in dichloroethane (19 mL) was stirred at room temperature for 20 minutes. Then, *N*,*N*′-bis(1-penthylhexyl)-perylene-3,4,9,10-tetracarboxydiimide (3.30 g, 4.72 mmol), *N*-iodosuccinimide (1.385, 5.65 mmol), $Cu(OAc)_2$ (426 mg, 2.34 mmol), and dichloroethane (122 mL) was added and the mixture was stirred at 80 °C for 1 day. After cooling, the solvent was evaporated and the residue was purified by column chromatography on silica gel eluted with dichloromethane/hexane (1:3, v/v) to give **1b** as a red solid (1.75 g, 45%): ^{1}H NMR (400 MHz, $CDCl_3$): δ 9.12 (s, 1H), 8.69–8.64 (m, 3H), 8.57 (d, *J* = 8.0 Hz, 1H) , 8.56 (d, *J* = 8.0 Hz, 1H), 8.52 (d, *J* = 8.0 Hz, 1H), 5.23–5.15 (m, 2H), 2.34–2.19 (m, 4H), 1.69–

1.83 (m, 4H), 1.44–1.23 (m, 24H), 0.86 (t, J = 6.8 Hz, 6H), 0.85 (t, J = 6.8 Hz, 6H); ^{13}C NMR (100 MHz, $CDCl_3$): 163.94, 163.86, 162.9, 162.1, 138.2, 137.9, 134.8, 134.2, 133.8, 133.0, 131.8, 131.6, 131.4, 130.9, 129.5, 126.42, 126.35, 124.3, 124.1, 124.0, 123.8, 123.4, 123.2, 123.0, 101.2, 55.6, 55.0, 32.5, 32.4, 31.8, 26.7, 22.5, 13.9; IR (KBr) ν = 1699, 1659 cm^{-1} (C=O); MP: 207.2–208.2 °C; HRMS (APCI) m/z calcd for $C_{46}H_{53}IN_2O_4$: $[M]^+$ 825.3128 Found: 825.3130.

2. Fabrication methods of organic devices

Fabrication and characteristics of OFET devices

dPTIa-, dPTIb-, IDT-PTIa–, and IDT-PTIb–based OFET devices were fabricated in a top-contact/bottom-gate (TCBG) configuration on a heavily doped n^+-Si (100) wafer with a 200 nm thermally grown SiO_2 (capacitance: C_i = 17.3 nF cm^{-2}). The substrate was treated with octadecyltrichlorosilane (ODTS) as reported previously.[4] The dPTIa- and dPTIb- thin films were fabricated by the spin-coating method (6000 rpm, 30 sec) using chloroform solution (4 g/L) and following thermal annealing (100 °C or 200 °C, 30 min). On the top of the organic thin film, gold films (80 nm) as drain and source electrodes were deposited through a shadow mask. For a typical device, the drain-source channel length (L) and width (W) are 40 μm and 1.5 mm, respectively. The device characteristics were measured at room temperature under ambient conditions with a Keithley 4200 semiconducting parameter analyzer. Field-effect mobility (μ) was calculated in the saturation regime using the following equation,

$$I_d = C_i \mu (W/2L) (V_g - V_{th})^2$$

where C_i is the capacitance of the SiO_2 insulator, and V_g and V_{th} are the gate and threshold voltages, respectively.

Fabrication and characterization of OPV devices

Patterned ITO substrates (purchased from Atsugi Micro) were first pre-cleaned sequentially by

sonicating in a detergent bath, de-ionized water, acetone, and isopropanol at room temperature, and in boiled isopropanol each for 10 min, and then baked at 120 °C for 10 minutes in air. The substrates were then subjected to a UV/ozone treatment at rt for 20 min. ZnO layer was prepared by spin-coating (at 5000 rpm, 30 sec.) a precursor solution prepared from zinc acetate dehydrate (0.27 g) and ethanolamine (0.07 mL) in 2-methoxyethanol (2.5 mL). Then, the substrates were annealed at 170 °C on a hot plate in air. The glass/ITO/ZnO substrate was transferred into a nitrogen-filled glove box (KOREA KIYON, KK-011AS-EXTRA). Active layer (IDT-PTI and PBDB-T) solution (chlorobenzene, 16 mg/ml, donor/acceptor weight ratio is 1:1) was spin-coated at 1200 rpm for 40 s on the substrate. Then, MoO_x (7.5 nm) and Ag anode (100 nm) were deposited in vacuum to complete the solar cell devices. The active area of the cells was 0.16 cm^2. *J-V* characteristics of the cells were measured using a Keithley 2400 source-measure unit in nitrogen atmosphere under the 1 sun (AM1.5G) condition using a solar simulator (SAN-EI Electric, XES-40S1). The light intensity was calibrated with a reference PV cell (KONICA MINOLTA AK-100 certified at National Institute of Advanced Industrial Science and Technology, Japan). The EQE of each device was measured with monochromatic light (SM-250F, Bunkoh-Keiki). More than 8 different devices were fabricated to collect the photovoltaic properties. AFM images were obtained on a Nanotechnology, Inc. scanning probe microscope Nanocute system. X-ray studies were carried out using a Rigaku Ultima IV diffractometer with a CuKα source (λ = 1.541 Å).

3. Absorption and fluorescence spectra of NDI and PDI

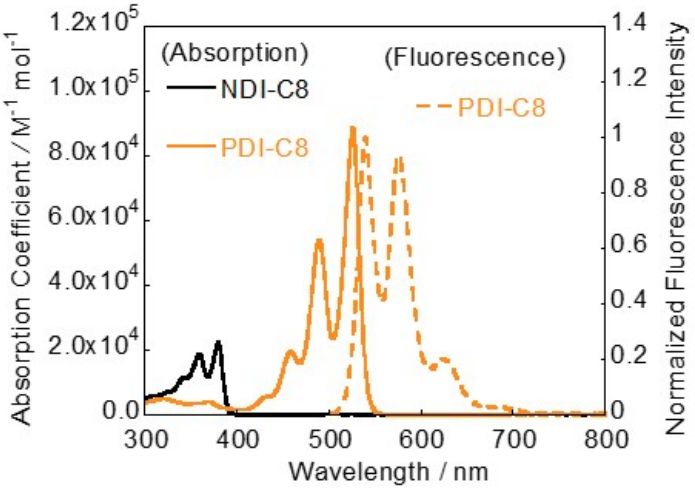

Figure S1. Absorption and fluorescence spectra of *N*,*N*′-dioctyl-NDI and *N*,*N*′-dioctyl-PDI in chloroform solution. *N*,*N*′-dioctyl-NDI did not show clear fluorescence.

4. Plausible mechanism of Na_2S-promoted thiophene annulation

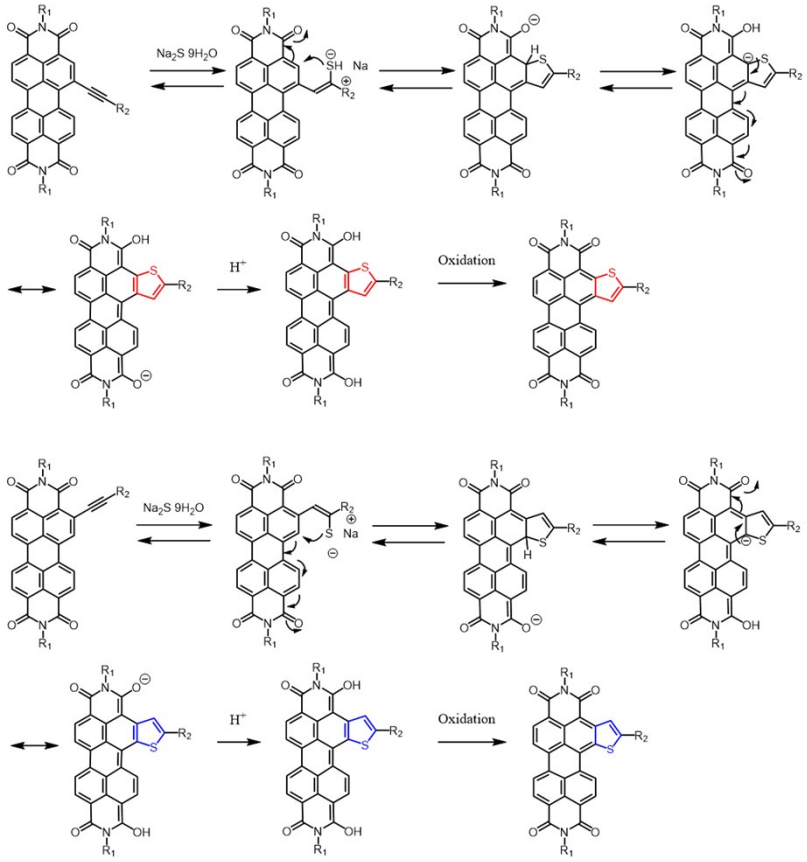

Figure S2. Plausible mechanism of Na_2S-promoted thiophene annulation on PDI-core from **2a** and **2b**.

5. Cyclic voltammograms

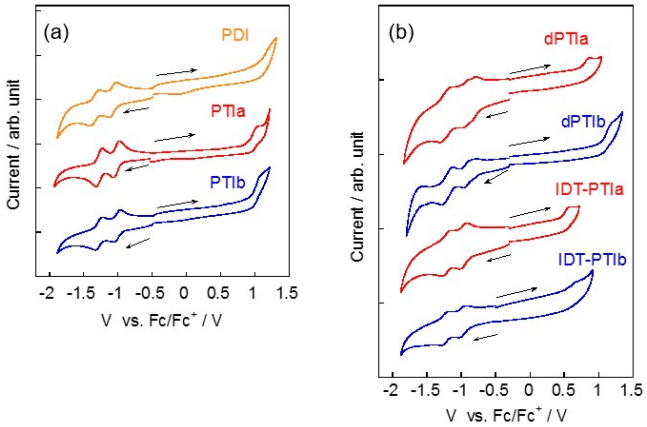

Figure S3. Cyclic voltammograms of PDI and PTIs (a) and dPTIs and IDT-PTIs(b)

6. Absorption spectra of dPTIs and IDT-PTIs in thin film

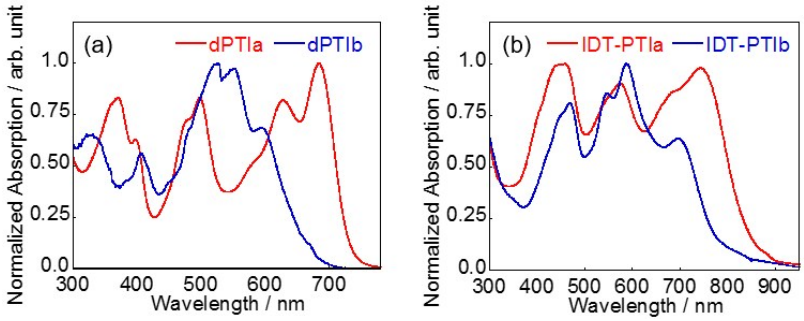

Figure S4. Absorption spectra of dPTIs (a) and IDT-PTIs (b) in thin film.

7. Logarithmic absorption spectra of dPTIs and IDT-PTIs

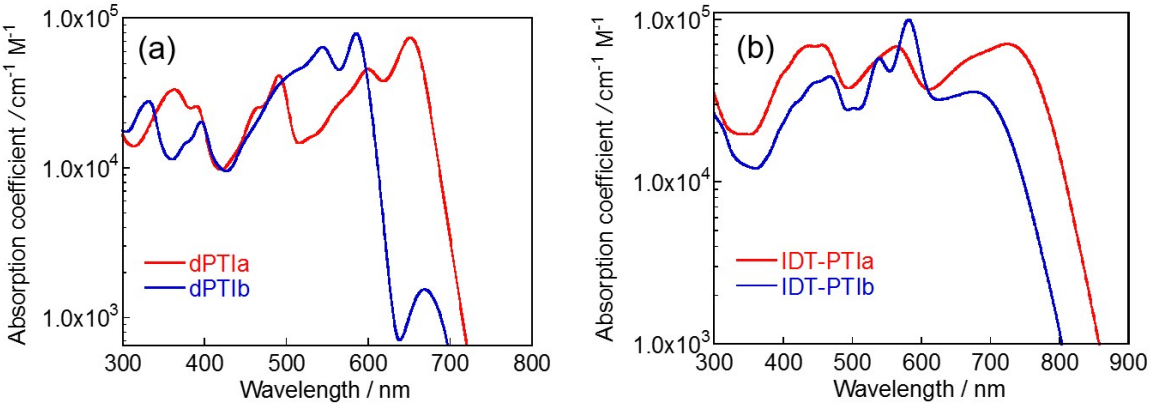

Figure S5. Logarithmic absorption spectra of dPTIs (a) and IDT-PTIs (b) in chloroform solution.

8. Dihedral angles of α,α′-linked thiophenes in the DFT-optimized molecular structures of dPTIs and IDT-PTIs

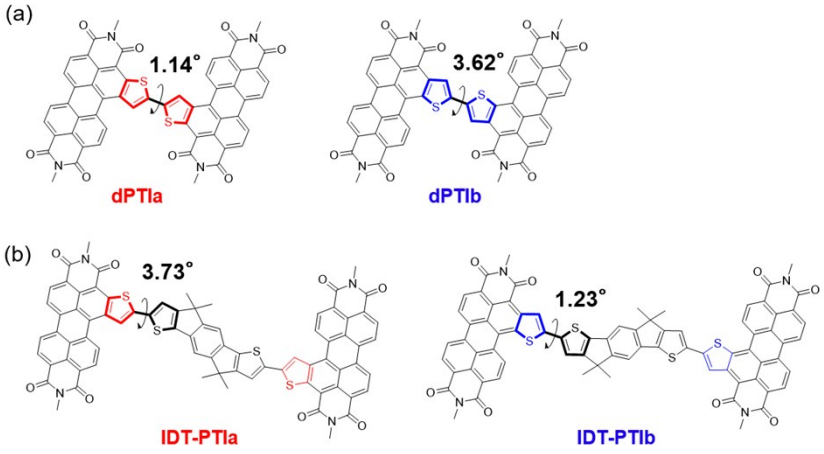

Figure S6. Dihedral angles of α,α′-linked thiophenes in the DFT-optimized molecular structures of dPTIs (a) and IDT-PTIs (b).

9. DFT-calculated HOMO and LUMO of PTIs

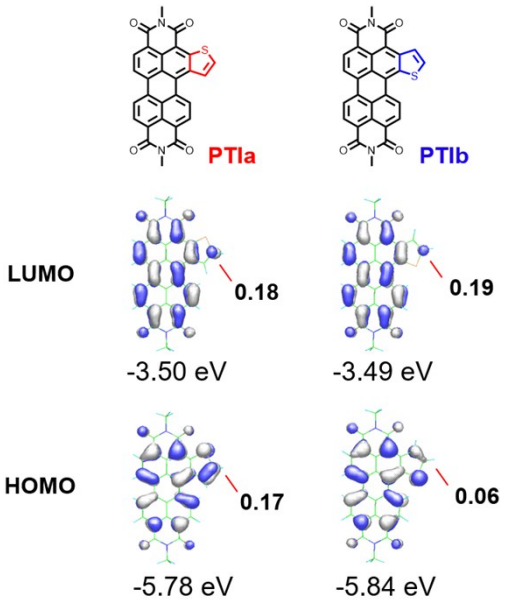

Figure S7. DFT-calculated HOMO and LUMO of PTIs and HOMO/LUMO coefficients at the α-carbon atoms of the fused thiophenes (B3LYP/6-31G*). The coefficients are given as absolute values.

10. AFM images

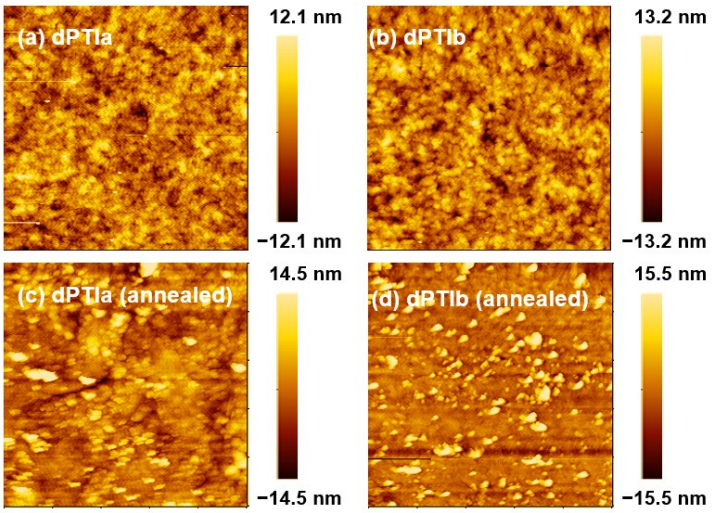

Figure S8. AFM images (5 μm × 5 μm) of dPTIa- and dPTIb-based OFETs with and without annealing (200 °C).

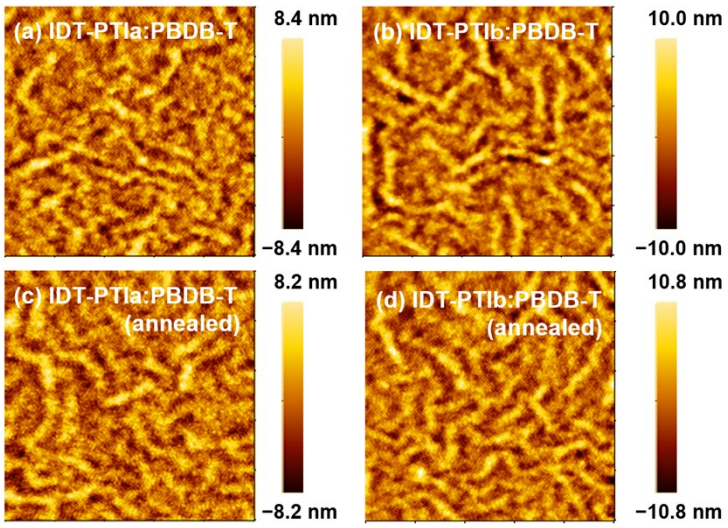

Figure S9. AFM images (5 μm × 5 μm) of IDT-PTIa:PBDB-T- and IDT-PTIb:PBDB-T-based OFETs with and without annealing (200 °C).

11. Out-of-plane and in-plane XRD patterns of thin-film of π-extended PTIs

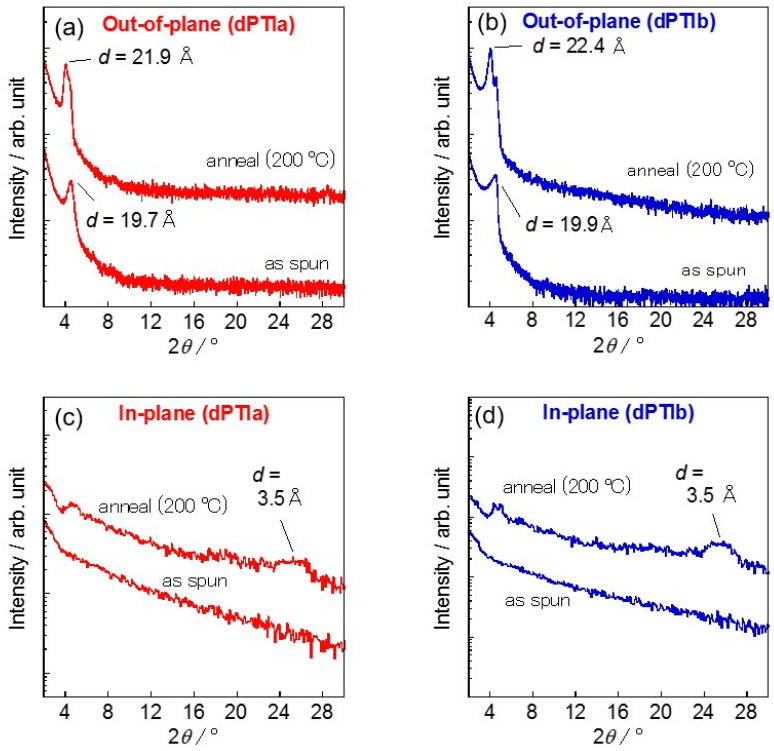

Figure S10. Out-of-plane XRD patterns of thin-film of dPTIa and dPTIb (a,b) and in-plane patterns of thin-film of dPTIa and dPTIb (c,d).

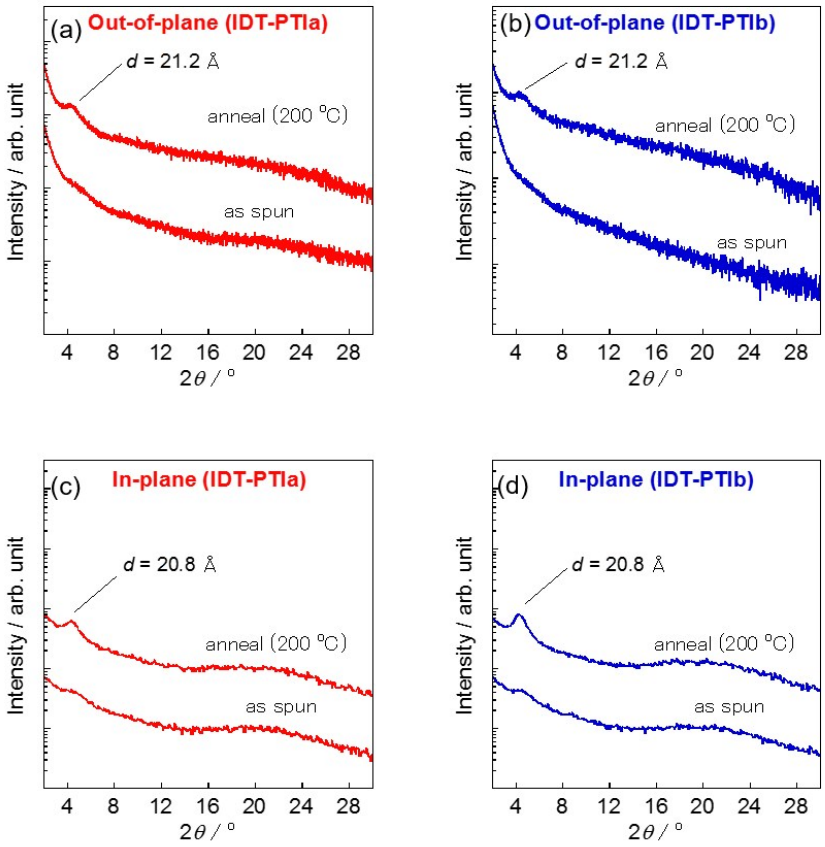

Figure S11. Out-of-plane XRD patterns of thin-film of IDT-PTIa and IDT-PTIb (a,b) and in-plane patterns of thin-film of IDT-PTIa and IDT-PTIb (c,d).

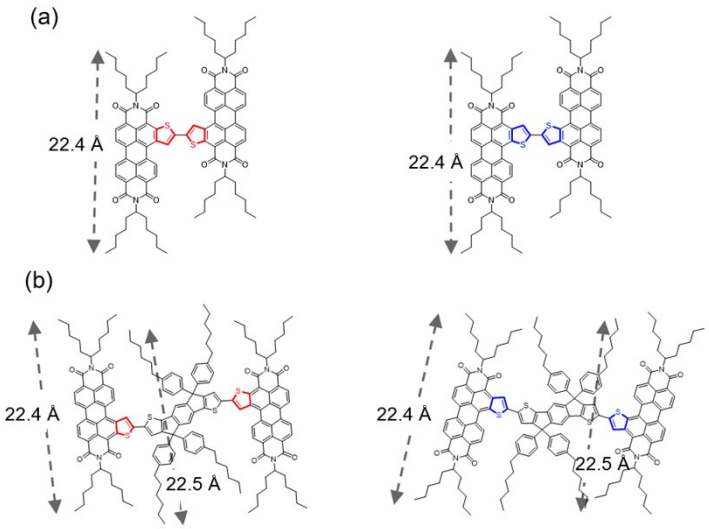

Figure S12. Molecular structures of dPTIs (a) and IDT-PTIs (b), and the distances between the edge of alkyl groups.

12. Evaluation of carrier mobilities of IDT-PTIs in the thin films by space-charge-limited current (SCLC) technique

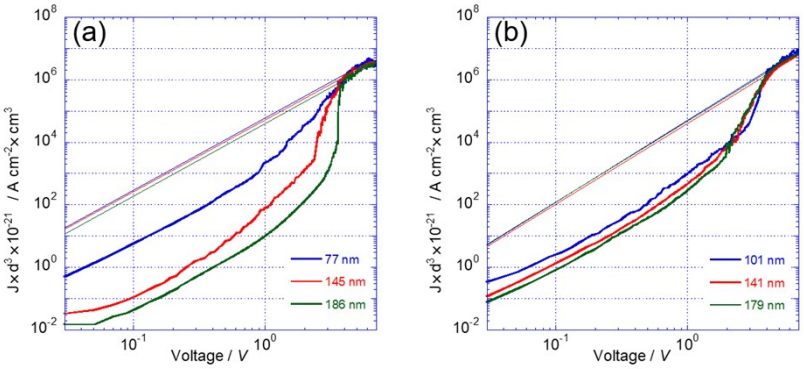

Figure S13. Current density normalized by the cube of the film thickness (*d*) plotted against voltage for the electron-only devices with the thin films of (a) IDT-PTIa and (b) IDT-PTIb (annealed at 200 °C). The device structures of electron-only devices are ITO/ZnO/Active layer/Ca/Ag.

Table S1. Summary of the average slope of *J-V* curves for analyzing he Mott-Gurney law, and the averaged electron mobility in SCLC region.

	IDT-PTIa	IDT-PTIb
Slope	2.29	2.57
μ_e / cm^2 V^{-1} s^{-1}	4.8×10^{-4}	4.2×10^{-4}

13. Out-of-plane and in-plane XRD patterns of thin-film of IDT-PTI:PBDB-T

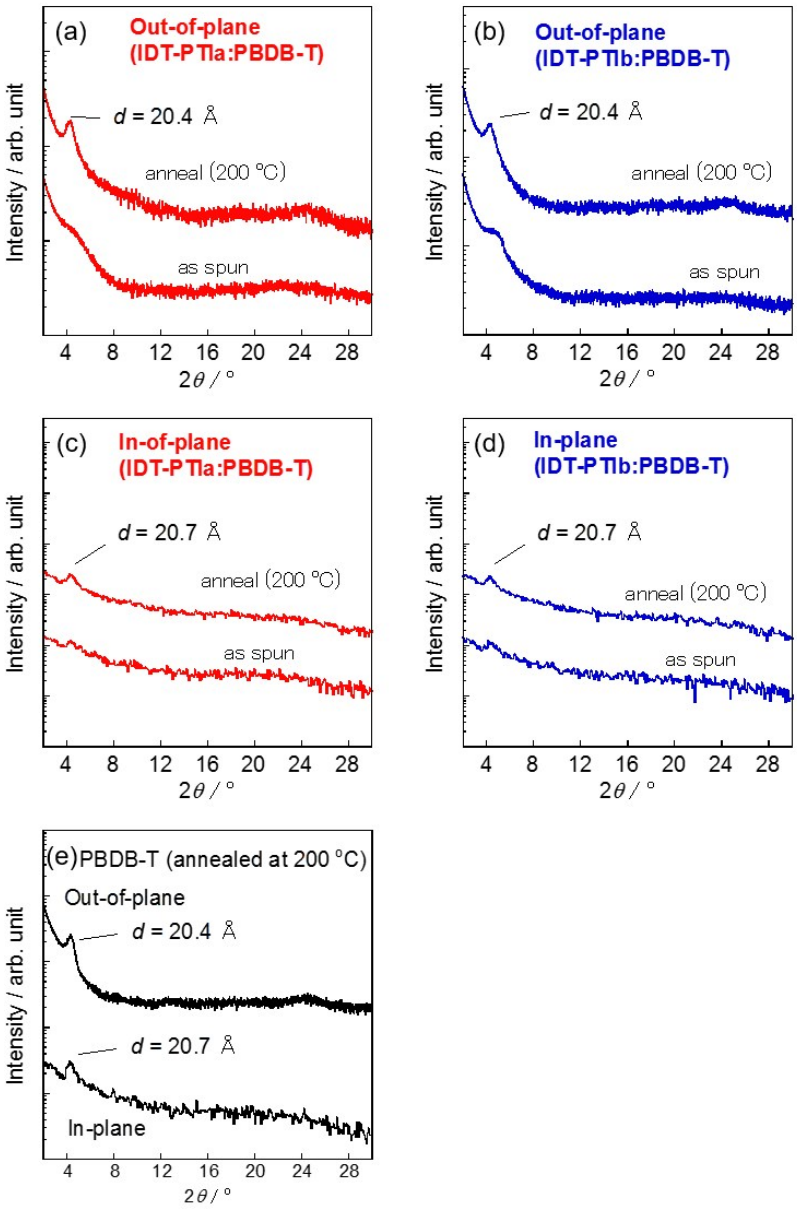

Figure S14. Out-of-plane XRD patterns of blend films of IDT-PTIa:PBDB-T and IDT-PTIb:PBDB-T and in-plane patterns of thin-film of IDT-PTIa:PBDB-T and IDT-PTIb:PBDB-T (c,d). XRD diffractions of PBDB-T (e).

14. Evaluation of carrier mobilities of blend films with IDT-PTIs:PBDB-T by SCLC technique

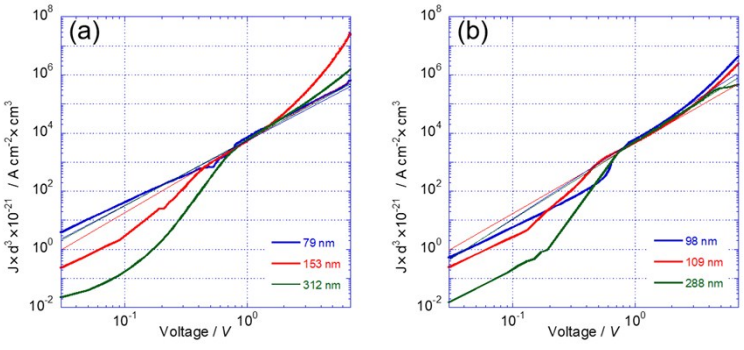

Figure S15. Current density normalized by the cube of the film thickness (*d*) plotted against voltage for the electron-only devices with the blend films of (a) IDT-PTIa:PBDB-T and (b) IDT-PTIb:PBDB-T. The device structures of electron-only devices are ITO/ZnO/Active layer/Ca/Ag.

Table S2. Summary of the average slope of *J-V* curves for analyzing he Mott-Gurney law, and the averaged electron mobility in SCLC region.

	IDT-PTIa:PBDB-T	IDT-PTIb:PBDB-T
Slope	2.28	2.62
μ_e / cm^2 V^{-1} s^{-1}	6.3×10^{-5}	5.3×10^{-5}

15. Summarized device characteristics

Table S3. Summarized transistor characteristics of dPTI-based OFETs

Compound	Anneal / °C	operation	μ_{FET} / $cm^2V^{-1}s^{-1}$	μ_{FET}^{max} / $cm^2V^{-1}s^{-1}$	I_{on}/I_{off}	V_{th} / V
dPTIa	–	n-channel	0.0092±0.0012	0.0104	~1.5×10^4	12.3±2.8
		p-channel	0.0004±0.0001	0.0005	~1.9×10^2	-44.2±2.9
	100	n-channel	0.0127±0.0041	0.0168	~1.5×10^3	10.1±5.2
		p-channel	0.0031±0.0009	0.0040	~3.4×10^2	-34.2±12.2
	200	n-channel	0.0882±0.0040	0.0922	~5.0×10^2	13.3±3.3
		p-channel	0.0198±0.0034	0.0232	~3.7×10^2	-22.5±5.4
dPTIb	–	n-channel	0.0070±0.0014	0.0084	~1.8×10^6	1.6±2.3
		p-channel	–	–	–	–
	100	n-channel	0.0167±0.0023	0.0190	~9.2×10^6	9.1±4.3
		p-channel	–	–	–	–
	200	n-channel	0.0378±0.0053	0.0431	~7.8×10^5	11.8±6.3
		p-channel	–	–	–	–

Table S4. Summarized properties of IDT-PTIa:PBDB-T– and IDT-PTIb:PBDB-T–based OPVs

Active Materials	*Anneal*	J_{SC} / $mAcm^{-2}$	V_{OC} / V	*FF*	*PCE* / %	PCE^{max} / %
IDT-PTIa:PBDB-T	-	8.60±0.42	0.83±0.01	0.49±0.02	3.2±0.6	3.8
	200	12.32±0.46	0.78±0.01	0.48±0.03	4.7±0.4	5.1
IDT-PTIb:PBDB-T	-	7.57±0.33	0.86±0.01	0.50±0.01	3.3±0.2	3.5
	200	10.06±0.45	0.82±0.00	0.56±0.02	4.7±0.2	4.9

16. NMR charts

N,*N*′-bis(1-penthylhexyl)-1-bromoperylene-3,4,9,10-tetracarboxydiimide (**1a**)

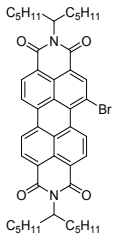

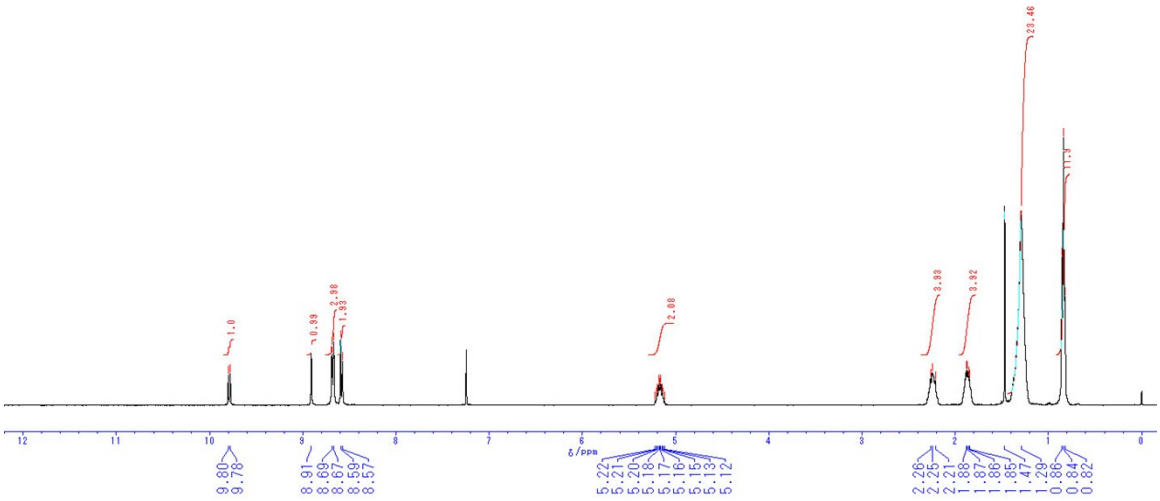

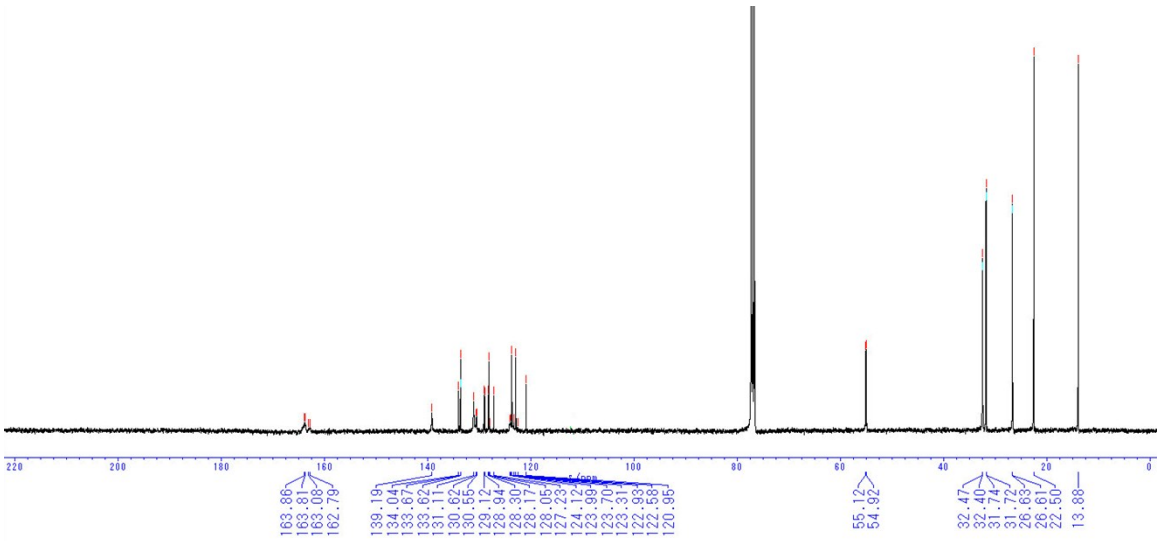

N,*N*′-Bis(1-pentylhexyl)-2-iodoperylene-3,4,9,10-tetracarboxydiimide (1b)

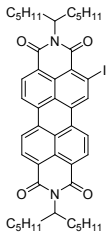

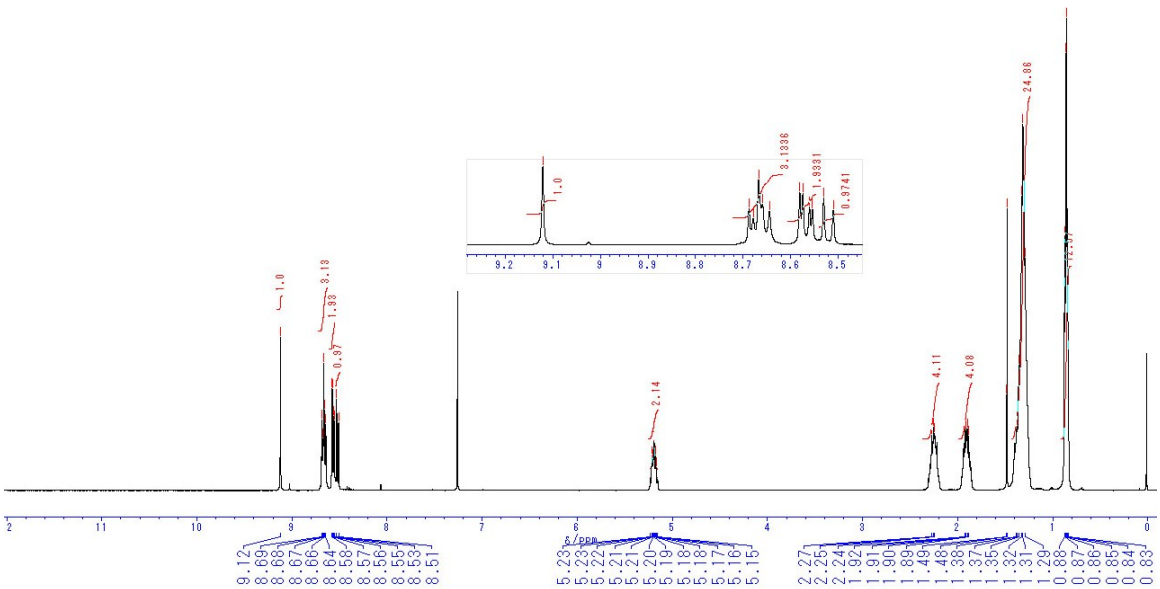

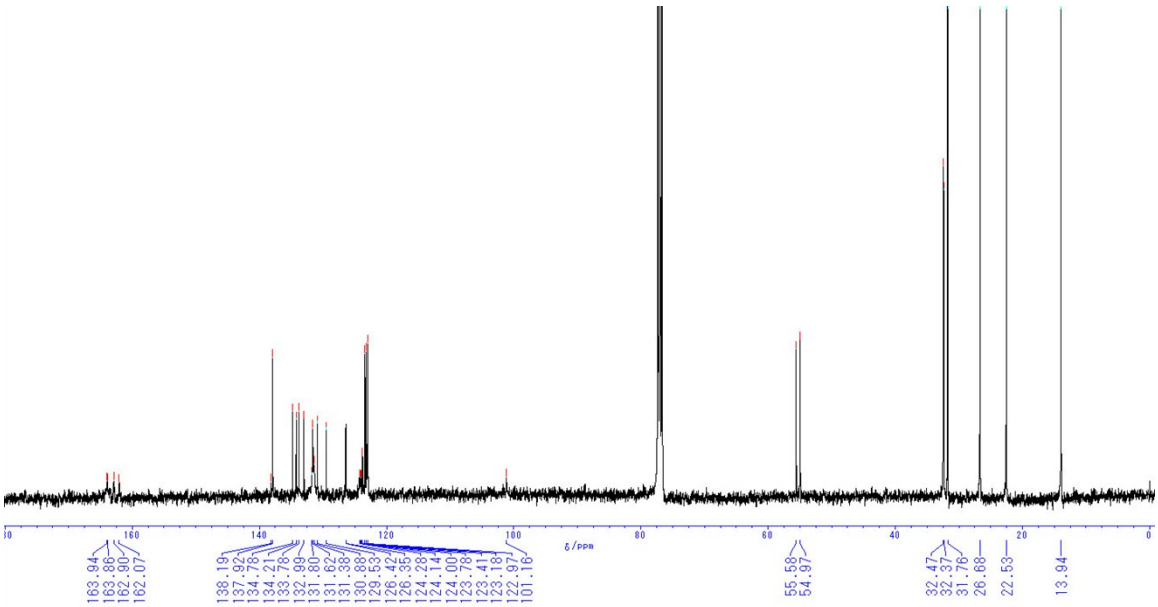

_N_,_N_′-Bis(1-pentylhexyl)-1-(triethylsilylethynyl)-perylene-3,4,9,10-tetracarboxydiimide (2a)

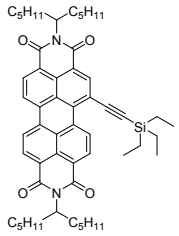

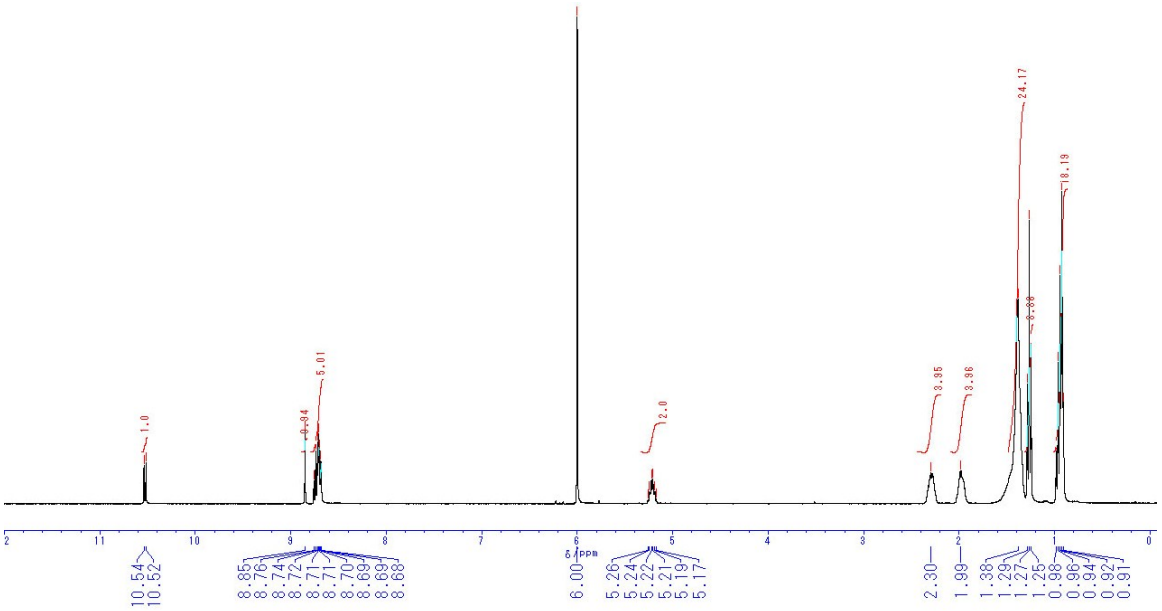

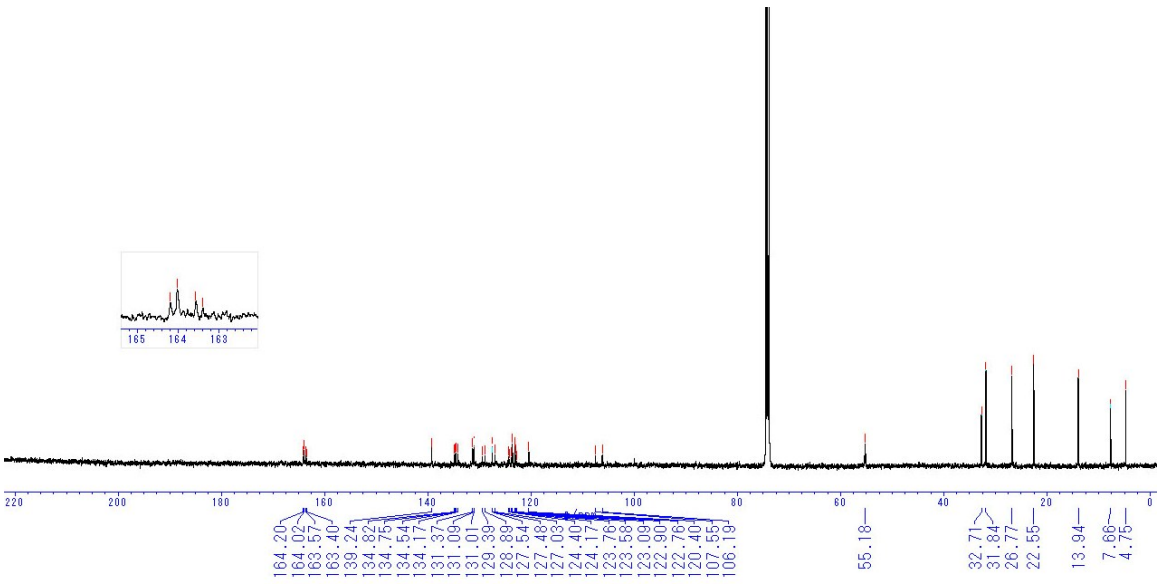

_N_,_N_′-Bis(1-pentylhexyl)-2-(triethylsilylethynyl)-perylene-3,4,9,10-tetracarboxydiimide (2b)

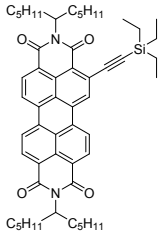

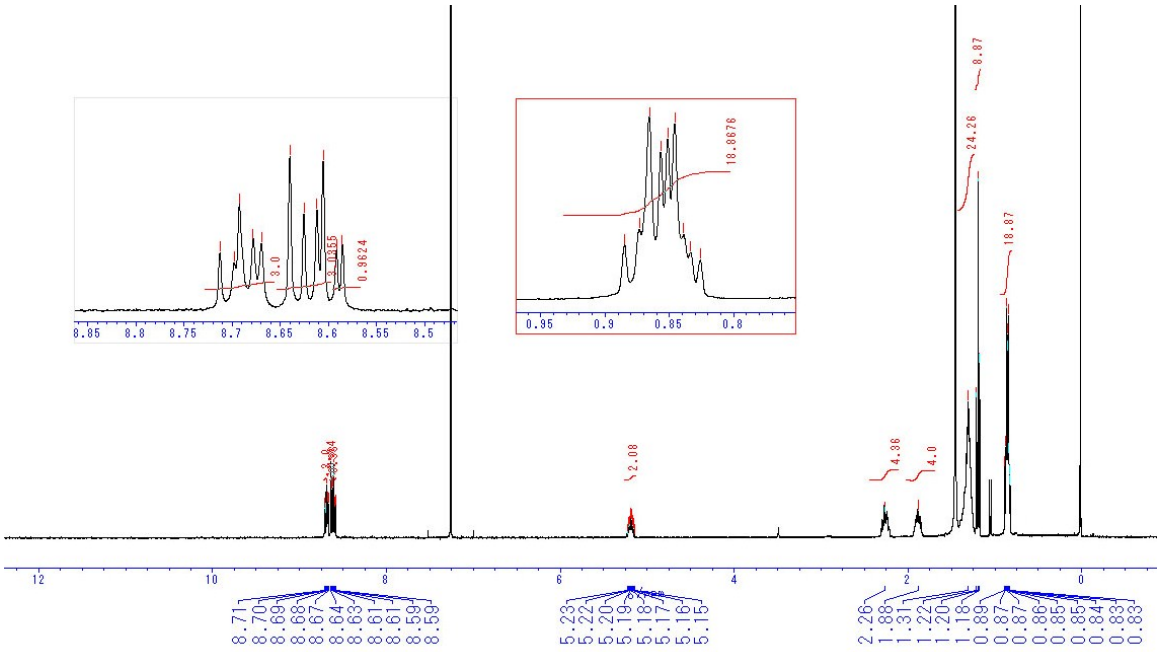

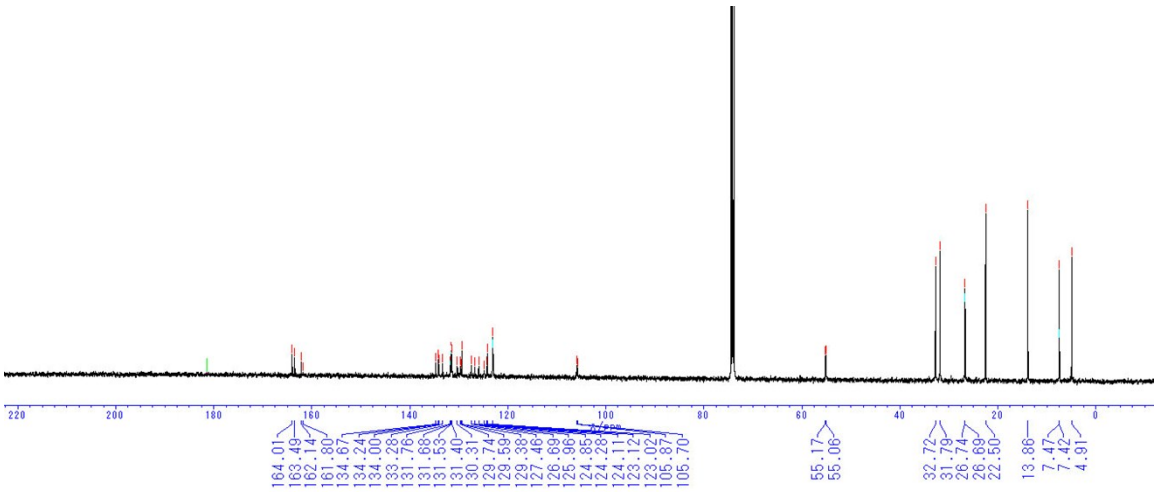

***N*,*N*′-Bis(1-pentylhexyl)-2-(triethylsilyl)-peryleno[2,1-*b*]thiophene-6,7,12,13-tetracarboxydiimide (TES-PTIa)**

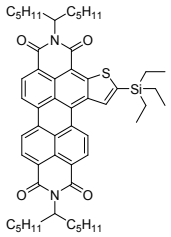

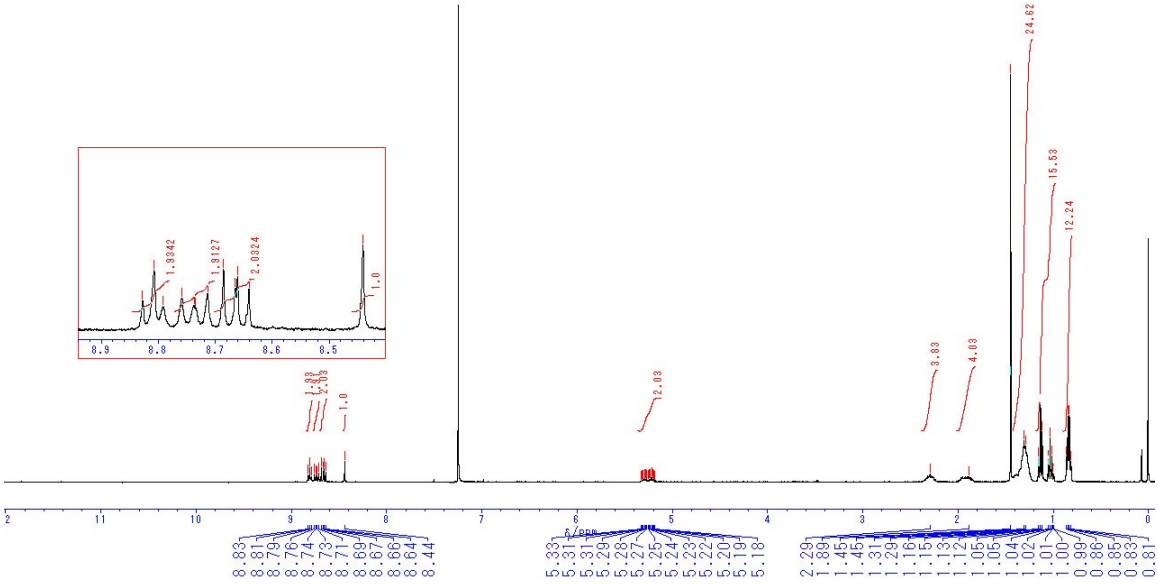

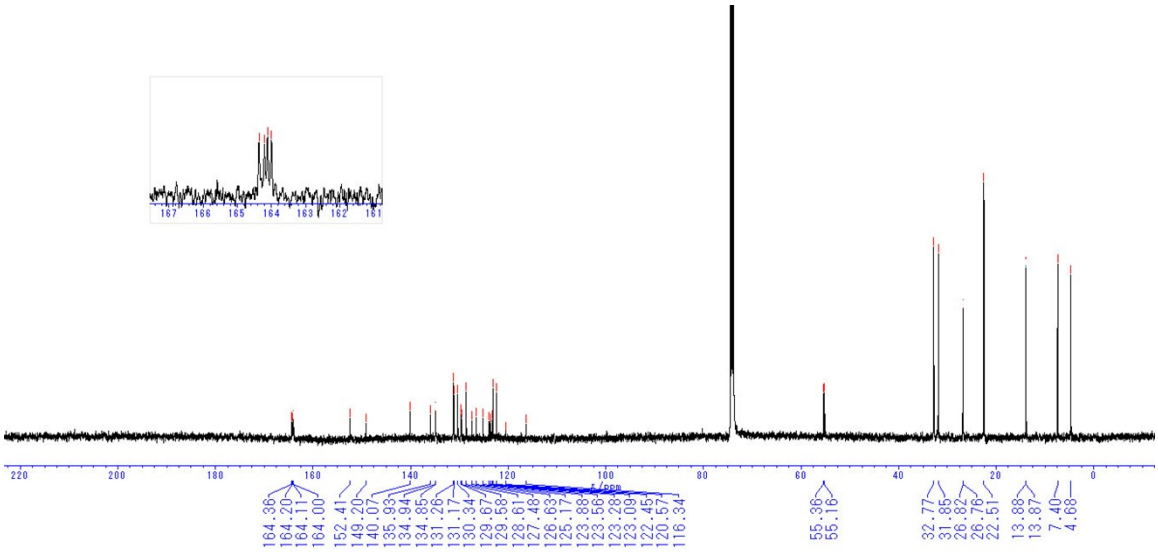

***N*,*N*′-Bis(1-pentylhexyl)-2-(triethylsilyl)-peryleno[1,2-*b*]thiophene-4,5,10,11-tetracarboxydiimide (TES-PTIb)**

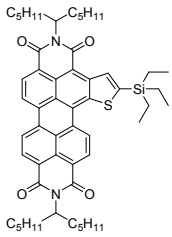

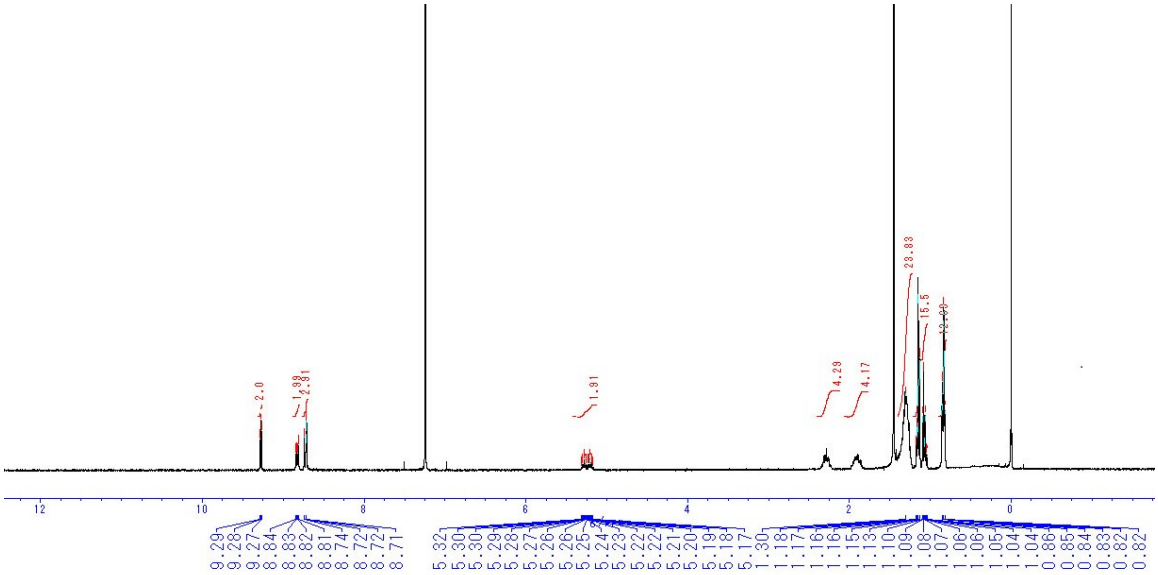

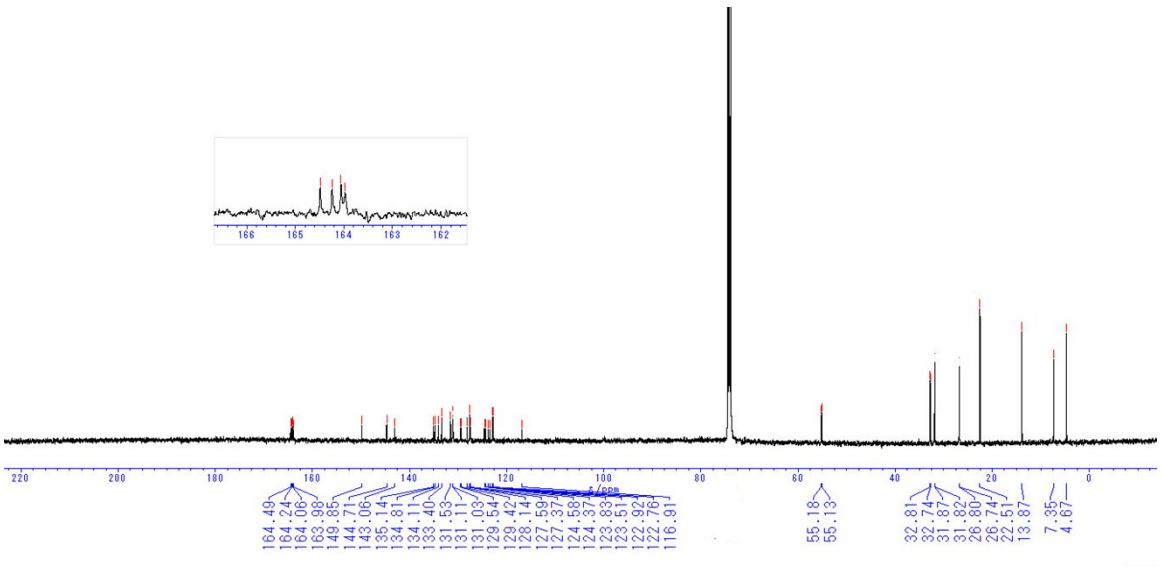

_N_,_N′_-Bis(1-pentylhexyl)-peryleno[2,1-_b_]thiophene-6,7,12,13-tetracarboxydiimide (PTIa)

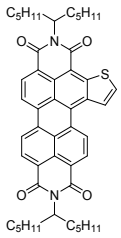

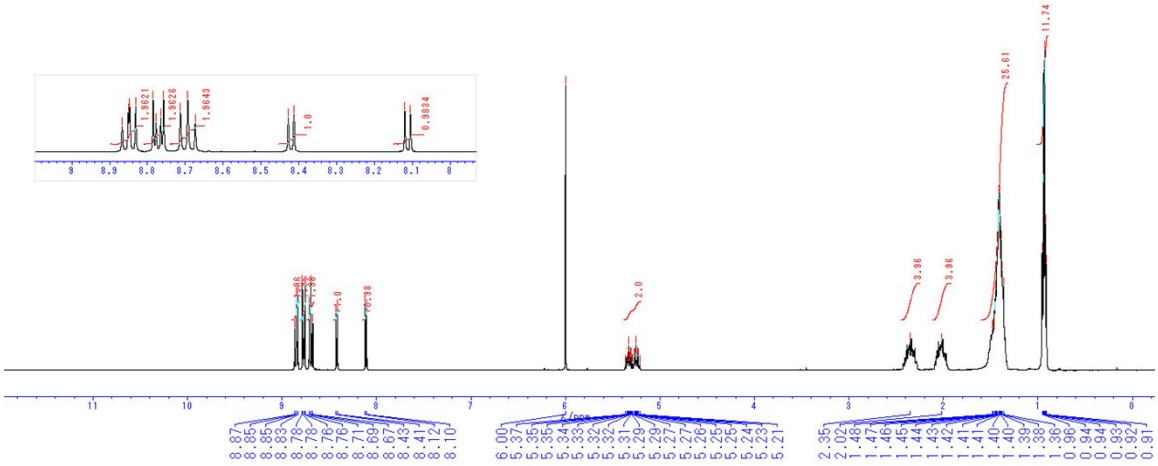

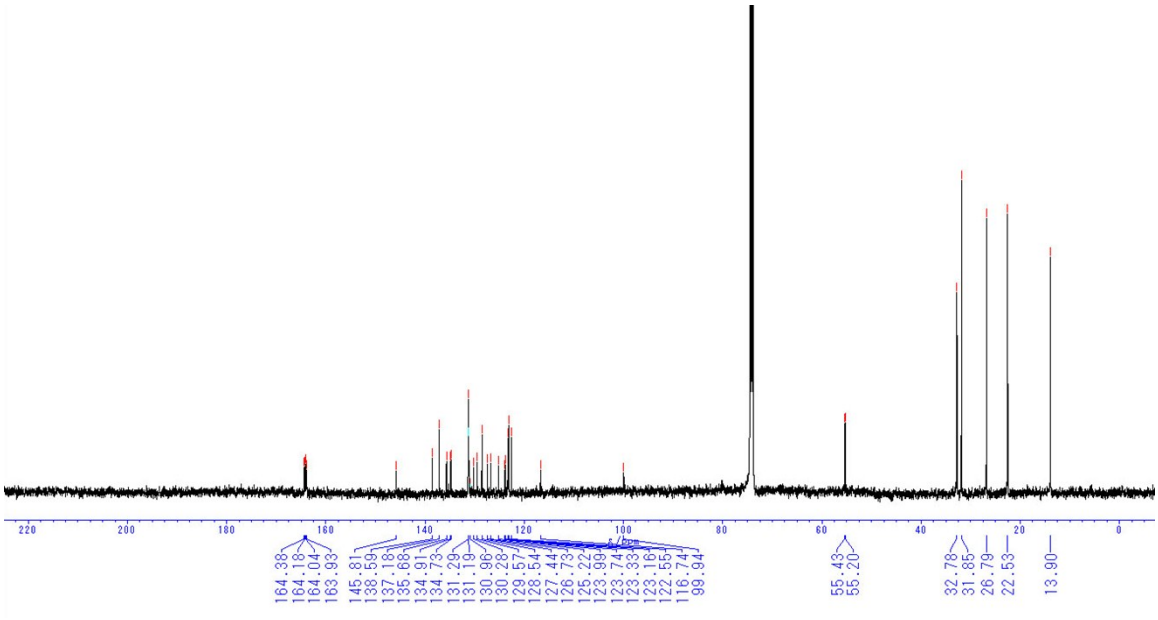

_N_,_N_′-Bis(1-pentylhexyl)-peryleno[1,2-_b_]thiophene-4,5,10,11-tetracarboxydiimide (PTIb)

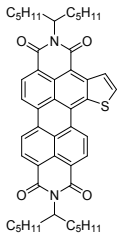

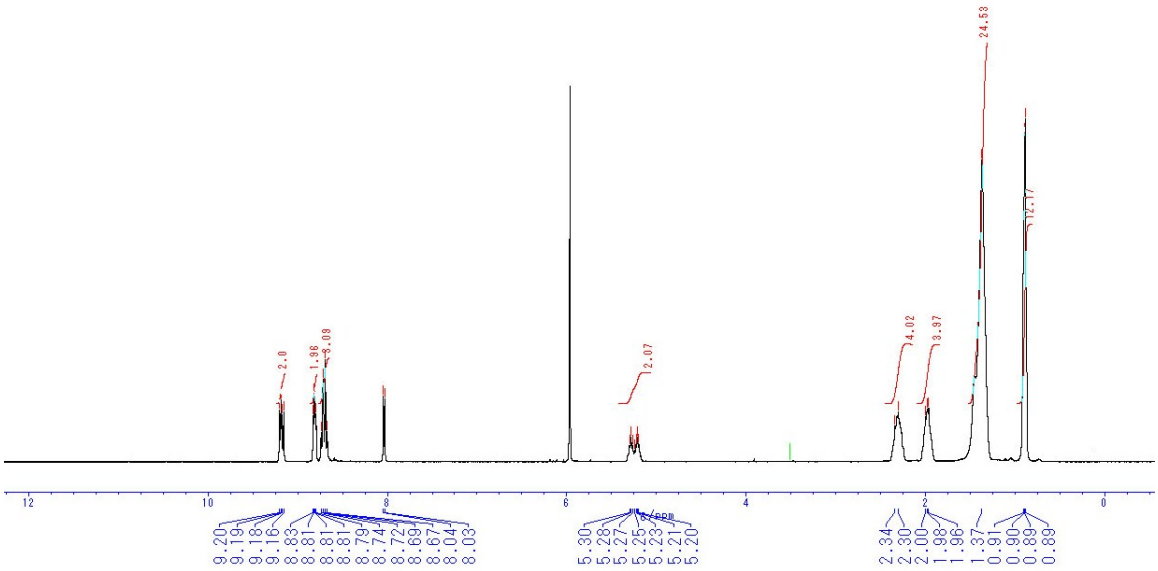

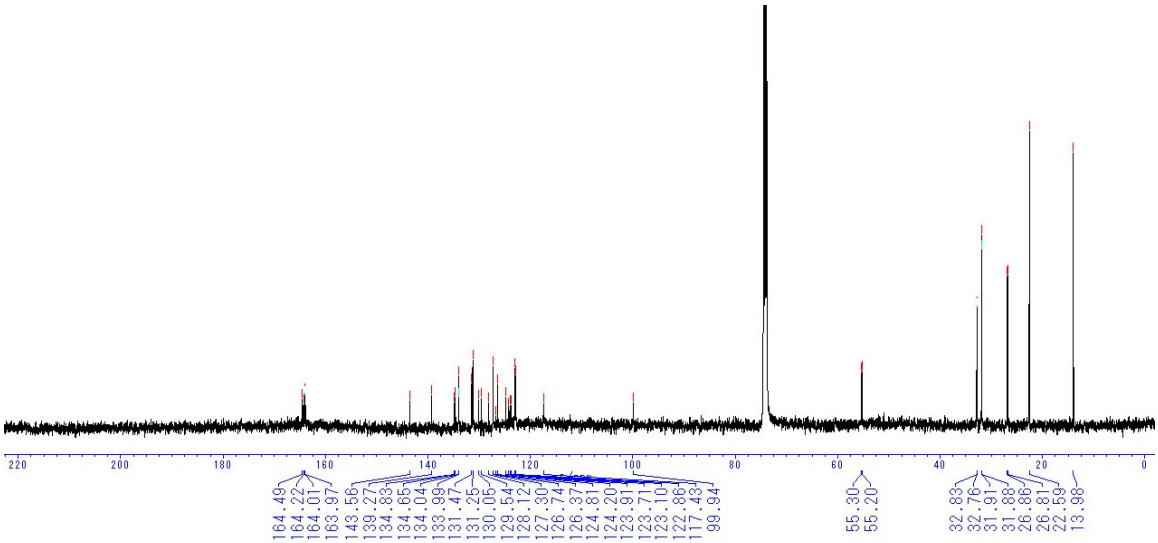

***N*,*N*′-Bis(1-pentylhexyl)-2-bromoperyleno[2,1-*b*]thiophene-6,7,12,13-tetracarboxydiimide (Br-PTIa)**

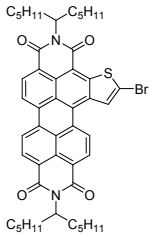

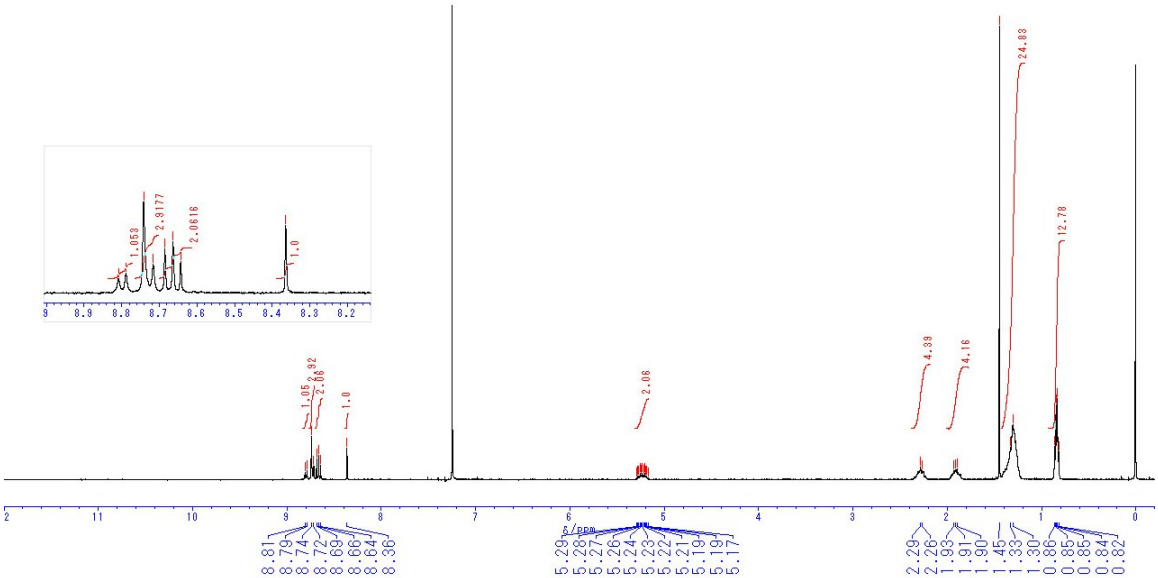

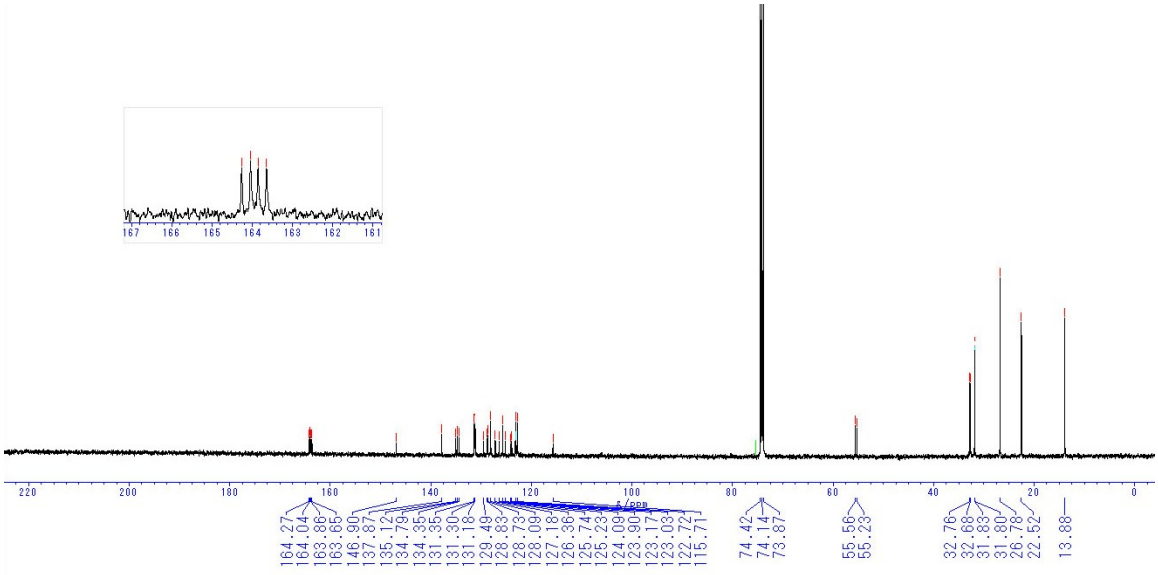

***N*,*N*′-Bis(1-pentylhexyl)-2-bromoperyleno[1,2-*b*]thiophene-4,5,10,11-tetracarboxydiimide (Br-PTIb)**

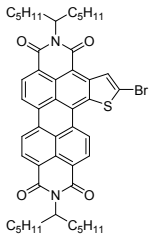

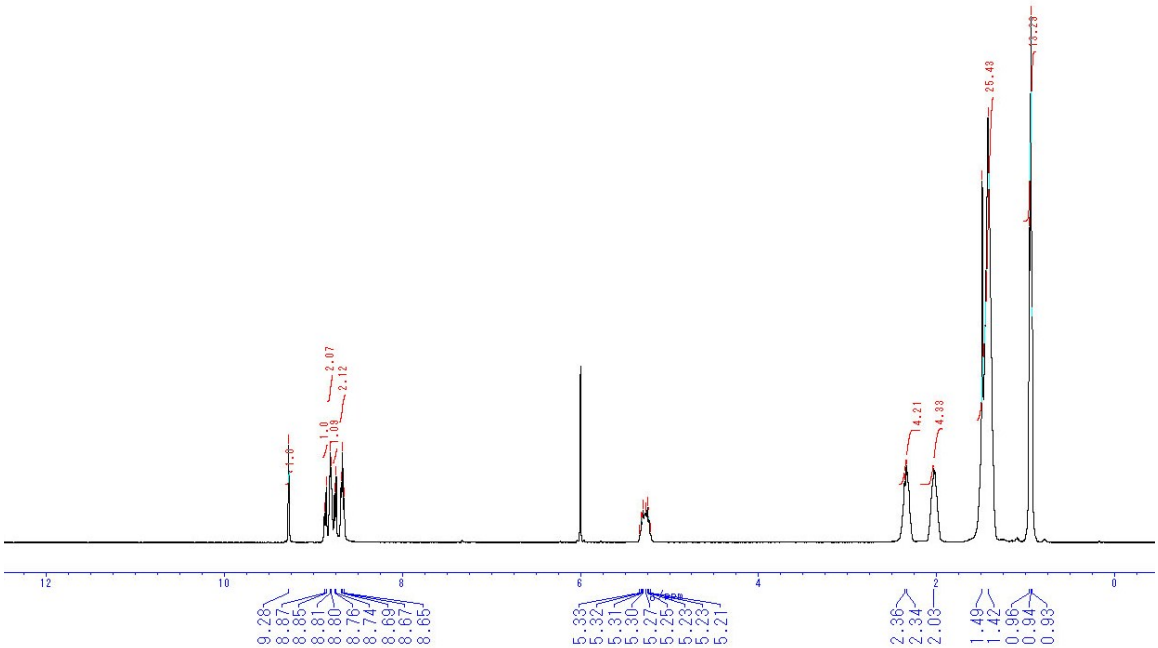

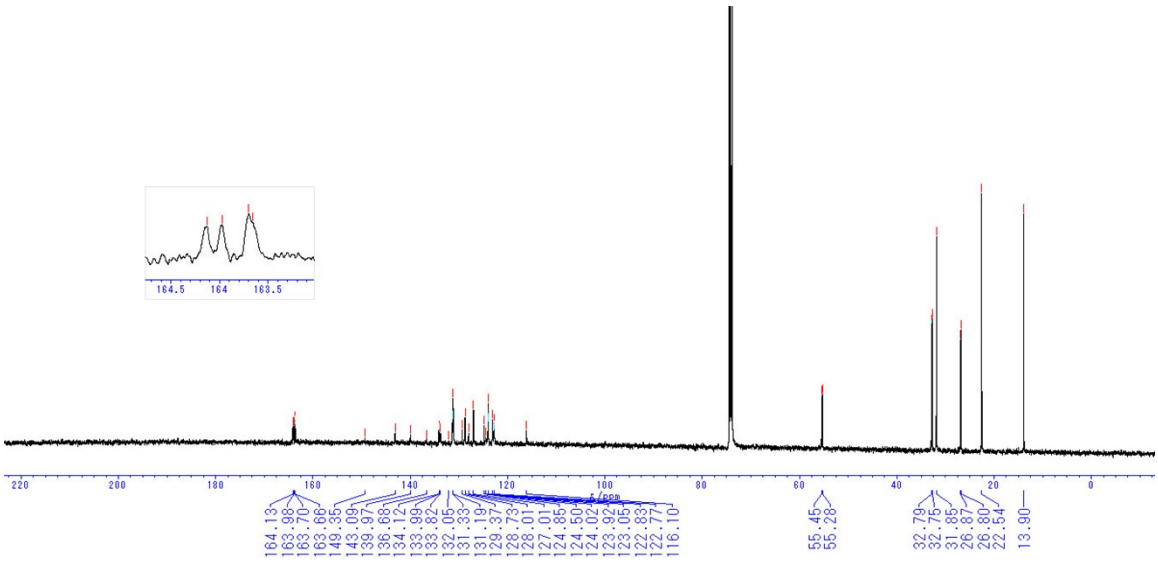

[2,2′]Bi[peryleno[2,1-*b*]thienyl]-*N*,*N*′,*N*″,*N*‴-tetrakis(1-pentylhexyl)-6,6′,7,7′,12,12′,13,13′-tetraimide (dPTIa)

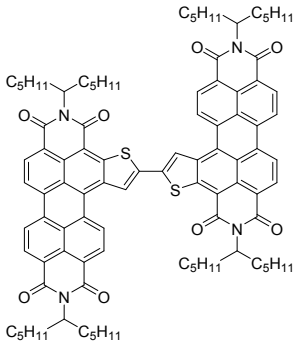

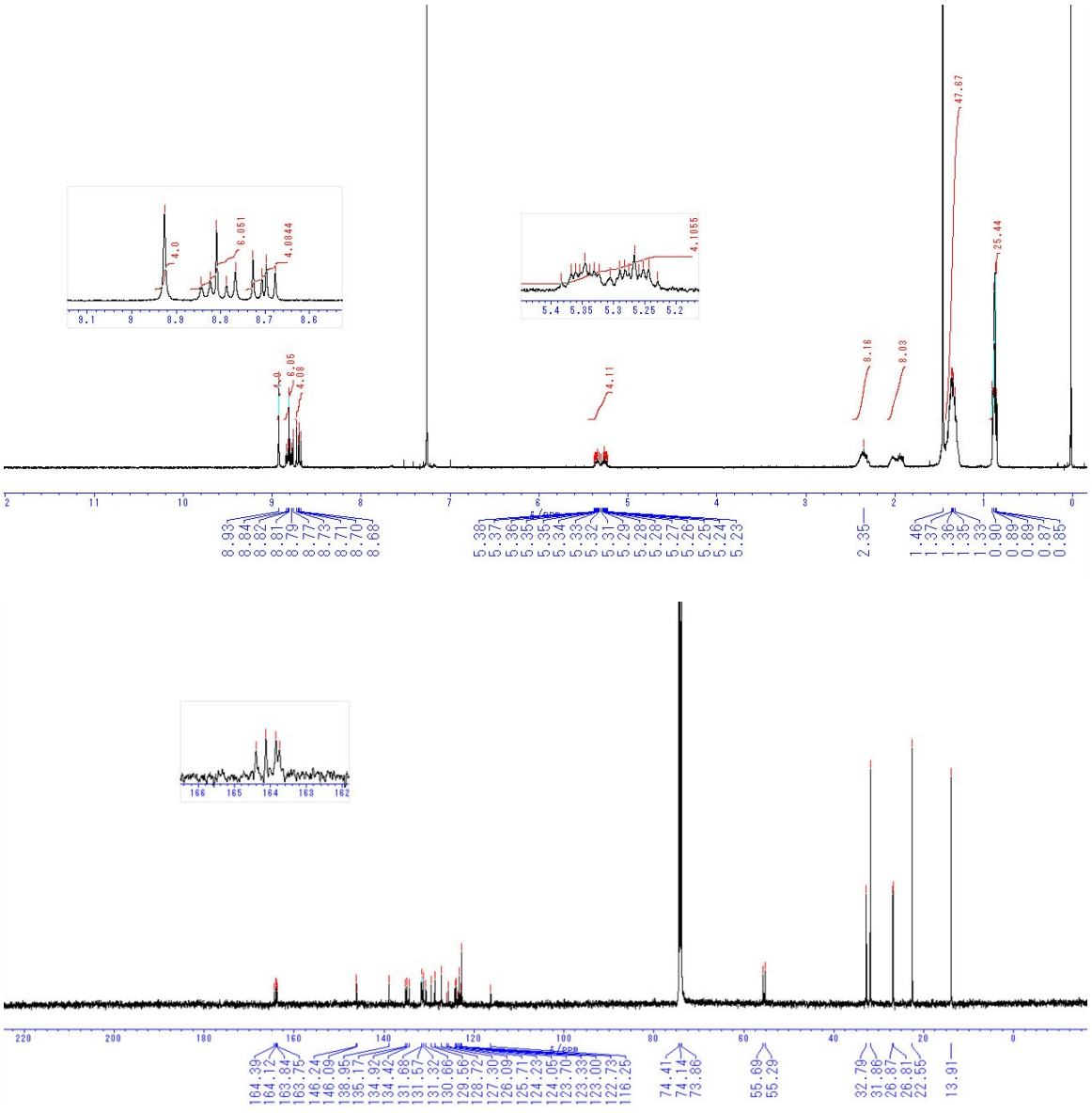

[2,2′]Bi[peryleno[1,2-*b*]thienyl]-*N*,*N*′,*N*″,*N*‴-tetrakis(1-pentylhexyl)-4,4′,5,5′,10,10′,11,11′-tetraimide (dPTIb)

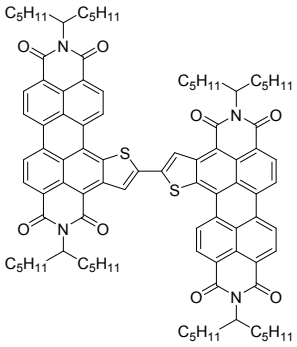

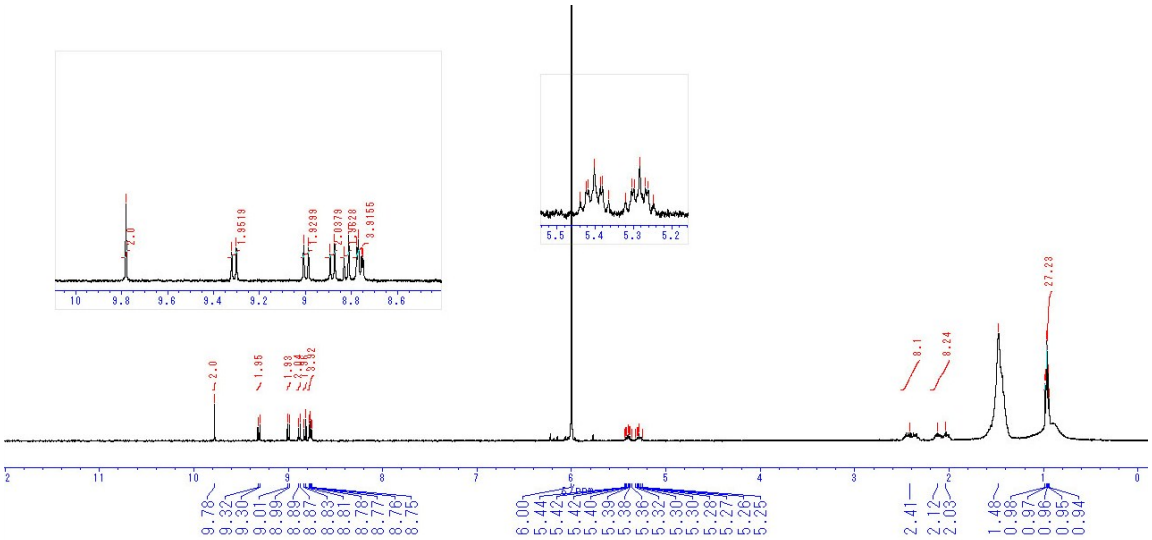

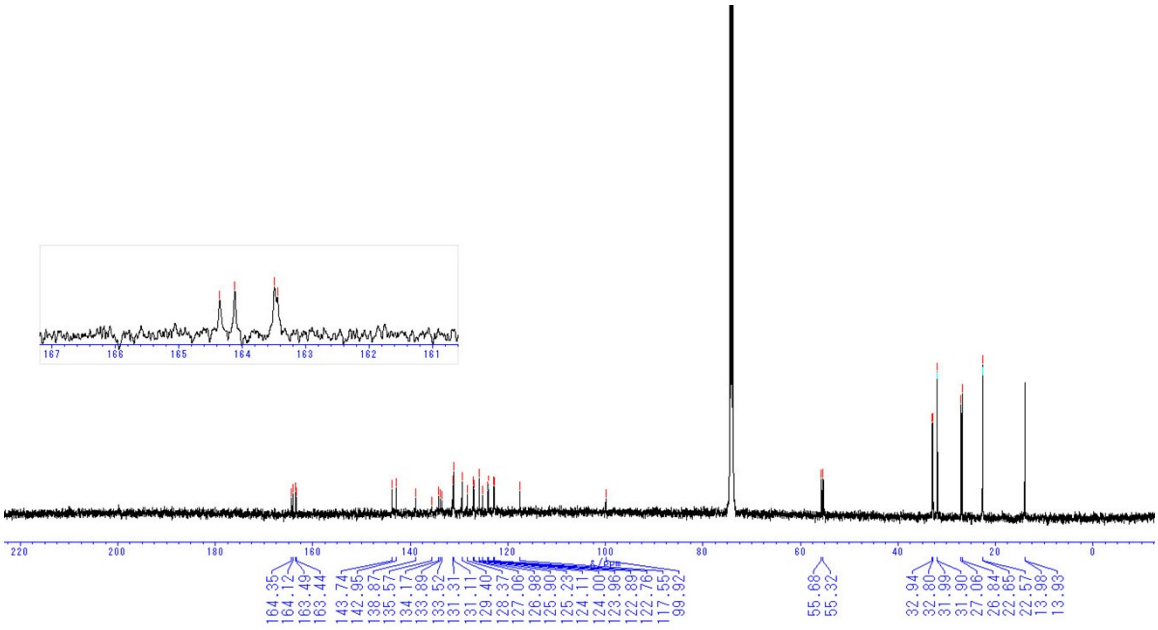

***N*,*N*′,*N*′′,*N*′′′-Tetrakis(1-pentylhexyl)-2,7-bis(peryleno[2,1-*b*]thiophen-2-yl)-4,4,9,9-tetrakis(4-hexylphenyl)-*s*-indaceno[1,2-*b*:5,6-*b*′]dithiophene-6′,6′′,7′,7′′,12′,12′′,13′,13′′-octacarboxytetraimide (IDT-PTIa)**

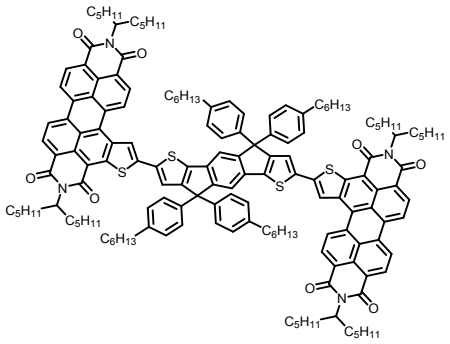

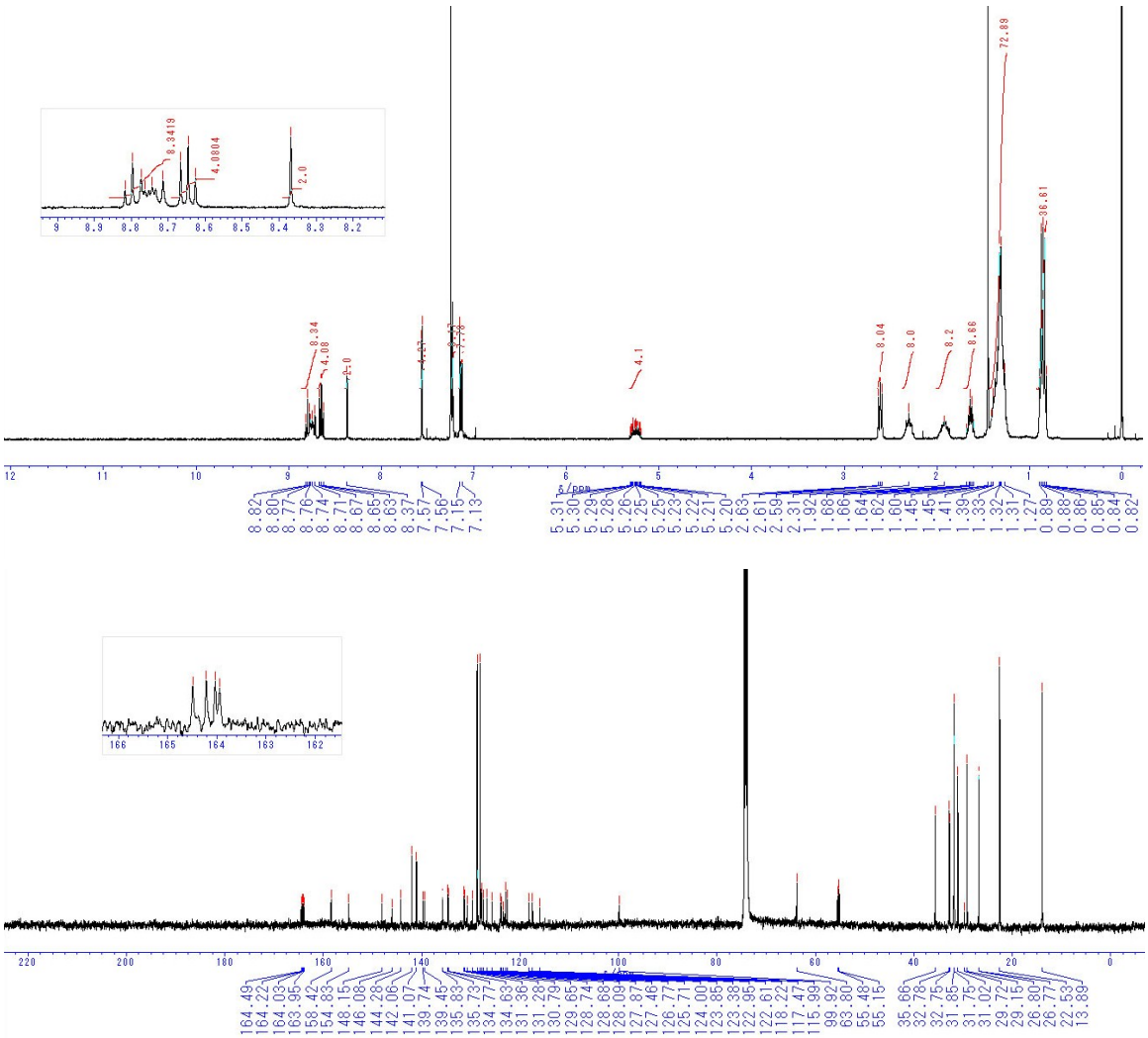

***N*,*N*′,*N*′′,*N*′′′-Tetrakis(1-pentylhexyl)-2,7-bis(peryleno[1,2-*b*]thiophen-2-yl)-4,4,9,9-tetrakis(4-hexylphenyl)-*s*-indaceno[1,2-*b*:5,6-*b*′]dithiophene-4′,4′′,5′,5′′,10′,10′′,11′,11′′-octacarboxytetraimide (IDT-PTIb)**

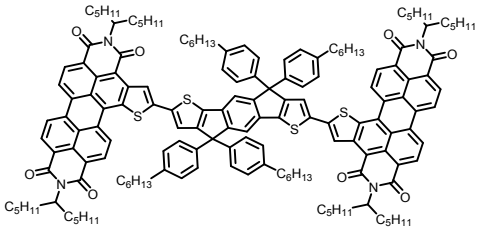

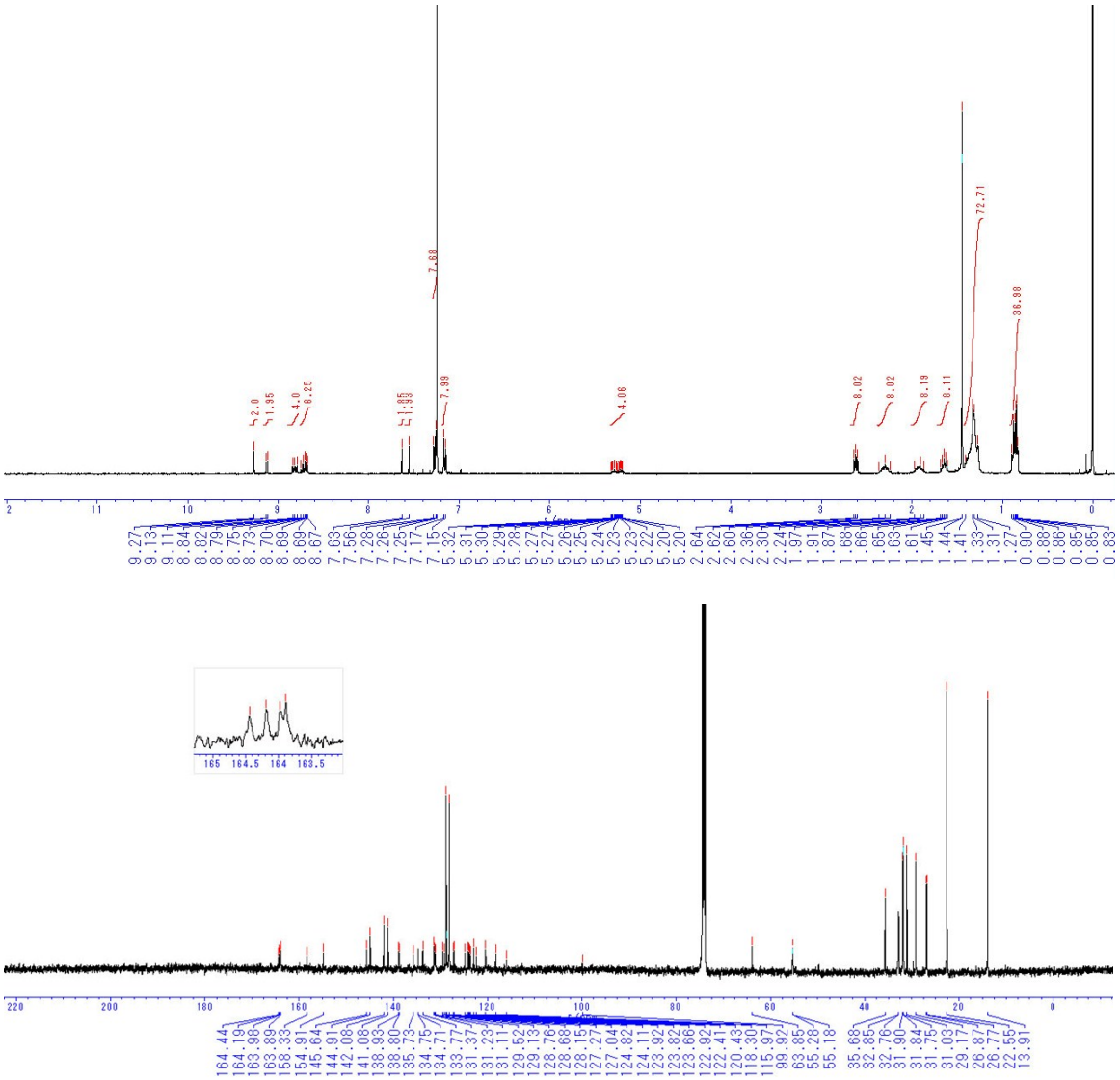

17. References

[1] P. Rajasingh, R. Cohen, E. Shirman, L. J. W. Shimon, B. Rybtchinski, *J.* Org. *Chem.,* 2007, **72**, 5973–5979.
[2] J. Jiajun, D. He, L. Zhang, Y. liu, X. Mo, J. Lin, H.-J Zhang, *Org. Lett.*, 2017, **19**, 5438–5441.
[3] N. V. Handa, K. D. Mendoza, L. D. Shirtcliff, *Org. Lett.,* 2011, **13**, 4724–4727.
[4] K. Takimiya, H. Ebata, K. Sakamoto, T. Izawa, T. Otsubo, Y. Kunugi, *J. Am. Chem. Soc.*, 2006, **128**, 12604–12605.